MreB5 Is a Determinant of Rod-to-Helical Transition in the Cell-Wall-less Bacterium Spiroplasma

Shrikant Harne, Sybille Duret, Vani Pande, Mrinmayee Bapat, Laure Béven, Pananghat Gayathri

MreB5 is a determinant of rod-to-helical transition in the cell wall-less bacterium *Spiroplasma*

Shrikant Harne[1], Sybille Duret[2], Vani Pande[1], Mrinmayee Bapat[1], Laure Béven[2*] and Pananghat Gayathri[1*]

[1.] Indian Institute of Science Education and Research, Pune, India 411008

[2.] INRAE, University of Bordeaux, Bordeaux, France

* Corresponding authors: Pananghat Gayathri, Laure Béven

Lead contact: Pananghat Gayathri

[1] Indian Institute of Science Education and Research Pune, Dr. Homi Bhabha Road, Pashan, Pune, India 411008. Phone: +91-20-25908128

[2] INRAE, University of Bordeaux, UMR 1332 BFP, Villenave d'Ornon, France. Phone: +33-6 23 78 20 13

Email: gayathri@iiserpune.ac.in, laure.beven@inrae.fr

Running title: Helical shape determination in *Spiroplasma*

Keywords: *Spiroplasma*, shape determination in cell wall-less bacterium, helical shape, MreB, fibril, cytoskeletal protein

Summary

In most rod-shaped bacteria, the spatial coordination of cell wall synthesis machinery and MreBs is the main theme for shape determination and maintenance in cell-walled bacteria [1–9]. However, how rod or spiral shapes are achieved and maintained in cell wall-less bacteria is currently unknown. *Spiroplasma*, a helical *Mollicute* which lacks cell wall synthesis genes, encodes five MreB paralogs and a unique cytoskeletal protein fibril [10,11]. Here we show that MreB5, one of the five MreB paralogs, contributes to cell elongation and is essential for the transition from rod-to-helical shape in *Spiroplasma*. Comparative genomic and proteomic characterization of a helical and motile wildtype *Spiroplasma* strain and a non-helical, non-motile natural variant helped delineate the specific roles of MreB5. Moreover, complementation of the non-helical strain with MreB5 restored its helical shape and motility by a kink-based mechanism described for *Spiroplasma* [12]. Earlier studies had proposed that length changes in fibril filaments are responsible for the change in handedness of the helical cell and kink propagation during motility [13]. Through structural and biochemical characterization, we identify that MreB5 exists as antiparallel double protofilaments which interact with fibril and the membrane, and thus potentially assists in kink propagation. In summary, our study provides direct experimental evidence for MreB in maintaining cell length, helical shape and motility, thus revealing the role of MreB in sculpting the cell in the absence of a cell wall.

Results and discussion

Early studies proposed a role for the cytoskeletal filaments fibril and MreB in morphogenesis and kinking motility of *Spiroplasma* [12,14,15]. The fibril protein does not have a homolog and is unique to the genus *Spiroplasma,* which also possess 5-7 paralogs of MreB [10,11]. A cytoskeletal ribbon, consisting of MreB and fibril filaments, positioned along the shortest helical path was proposed to drive changes in handedness of the helical cell of *Spiroplasma*, leading to kinking motility [15–17]. However, experimental evidence demonstrating functions of fibril and the multiple MreB paralogs in *Spiroplasma* physiology is unavailable, mainly due to limited tools for disruption of target genes.

Our pursuit towards understanding fundamental mechanisms of achieving cell shape led us to a comparative genomic and proteomic characterization of the wildtype helical and motile strain *Spiroplasma citri* GII-3 (hereafter referred to as GII-3) and a natural variant, ASP-I, which is non-helical and non-motile [18]. The pair serves as an ideal model system to understand the molecular basis of helicity in Spiroplasmas. A previous study on comparison of semi-purified membrane fractions of *S. citri* SP-A (wildtype; helical and motile) and ASP-I cells revealed an unidentified protein of about 39 kilodalton (kDa) of unknown function to be missing from the latter [18].

Motile GII-3 cells exhibit translational motility on soft agar and form diffuse colonies, in contrast to compact colonies formed by the non-motile ASP-I [19], which can be clearly differentiated using Dienes' stain (Figure 1A) [20]. In electron micrographs, the GII-3 cells were helical while ASP-I cells were rod shaped (Figure 1B). To quantify cell helicity, we measured the ratio of the cell contour (L1) and the

shortest distance between two points along its body length (L2). For a perfect rod, the L1/L2 ratio will be 1 and deviation from this value (> 1) indicates bent/curved/helical shapes. We observed the mean L1/L2 ratio for GII-3 and ASP-I cells to be 1.25 ± 0.12 and 1.07 ± 0.05, respectively [mean ± SD (standard deviation); Figure 1C]. Additionally, we differentiated between bent and helical cells based on the number of crossovers between the paths of L1 and L2. For a helix, the path L1 will cross L2 (shortest path) at least once whereas, the path L1 of a curved or a bent cell need not cross L2. GII-3 and ASP-I cells showed mean values of 1.85 ± 0.42 and 0.06 ± 0.18 crossover/µm of L2 (mean ± SD; Figure 1D), respectively. The two strains possessed similar widths (108.9 ± 1.3 nm and 100.6 ± 1.1 nm for GII-3 and ASP-I respectively; Figure 1E). Some of the ASP-I cells exhibited a branched morphology (marked by *, Figure 1B), while some appeared bulged at the tip (marked by #, Figure 1B), both features were not observed in the GII-3 images. Thus, we established that the two strains used in our study were morphologically different, with GII-3 exhibiting a characteristic helical shape and ASP-I cells being rod shaped.

To investigate if fibril and/or MreB proteins have been affected in the ASP-I strain, corresponding genes from GII-3 and ASP-I genomes were sequenced. The pair-wise sequence alignment of *fibril* and *mreB* sequences revealed that the proteins encoded by fibril and MreB1 to MreB4 were intact in both cell types. However, a point mutation was observed in *mreB5* gene of ASP-I cells at the 400th nucleotide (Figure 1F, Figure S1). The mutation (G → T) results in a stop codon (TAG) after 133 amino acids, resulting in a truncated MreB5 protein in ASP-I cells instead of the 352-amino-acid wildtype MreB5 protein (38.5 kDa). Whole genome sequencing of ASP-I strain (reference number PRJNA635252) confirmed the point

mutation in *mreB5* and the absence of additional *mreB* sequences other than *mreB1-5* in the genome.

Further, we performed mass spectrometry analysis of trypsinized samples of the cytosolic and membrane/Triton X-114 solubilized fractions from the two cell types. The peptide fragments of all MreBs, including MreB5 were found in both cytosolic and membrane fractions of wildtype (GII-3) cells (Figure 1G). However, no MreB5 peptides were detected in the cytosolic fractions of ASP-I cells while two peptides corresponding to a 4.6 % coverage of MreB5 were detected at very low abundance in the membrane fraction (Figure 1G; bar corresponding to MreB5 is not seen because it lies below the displayed y-axis range).

To demonstrate that the absence of a functional MreB5 is responsible for the altered phenotype of ASP-I cells, we performed vector-based expression of wildtype *mreB5* under *ef-Tu* (*tuf*) promoter in the ASP-I cells. Polymerase chain reaction (PCR)-based controls proved that the transformants were indeed ASP-I cells carrying pSD4 vector (Figure S2A). Consistent with the colony morphology of non-motile ASP-I (Figure 1A, right) [19], the ASP-I cells transformed with empty pSD4 vector (*S. citri* ASP-I^{pSD4}) formed compact colonies (Figure 2A, top). The ASP-I cells expressing wildtype *mreB5* (*S. citri* ASP-I^{MreB5}) displayed a diffuse colony morphology (Figure 2A, bottom) similar to motile GII-3 cells (Figure 1A, left) [19]. This indicated that the expression of wildtype *mreB5* enabled translational motility in *S. citri* ASP-I cells.

Dark field microscopy observations revealed that the GII-3 cells showed helical morphology and kinking motility (Video S1; Figure 2B). ASP-I cells were rod-shaped and non-motile (Video S2), while ASP-I^{MreB5} cells were helical and motile

(Video S3), similar to the wildtype (GII-3) cells (Figure 2B). We found that the ASP-I^{MreB5} cells moved with a mean velocity of 4.16 ± 0.78 µm/sec analogous to GII-3 cells (3.59 ± 0.99 µm/sec) (Figure 2C). The ASP-I cells were non-motile (0.02 ± 0.04 µm/sec; Figure 2C; mean ± SD) and exhibited erratic twitching/flexing movements only (Video S2).

Expression of a full-length MreB5 protein in ASP-I cells resulted in a helical shape, similar to that of wildtype (GII-3) cells. Mean ratio of cell contour length (L1) to the shortest distance between cell poles (L2) for the three cell types in exponential phase were 1.35 ± 0.13 (GII-3), 1.26 ± 0.12 (ASP-I^{MreB5}) and 1.07 ± 0.06 (ASP-I) (Figure 2D), consistent with the observed helical cells of GII-3 and ASP-I^{MreB5}. In late exponential phase, mean L1/L2 ratio of GII-3 (1.09 ± 0.10) as well as ASP-I^{MreB5} (1.15 ± 0.15) cells decreased to ~ 1, indicating a loss of helicity for both cell types (Figure 2D).

Typically, an MreB is known for its role in cell elongation. To check if the absence of MreB5 affects cell length in *S. citri*, we estimated the contour length L1 of the cell types at equivalent stages of exponential and late exponential growth phases. In exponential phase, the mean length of ASP-I cells (2.35 ± 0.62 µm) was shorter than that of GII-3 (6.21 ± 2.02 µm) and ASP-I^{MreB5} (5.26 ± 2.37 µm) (Figure 2E). In late exponential phase, the mean cell lengths observed were 2.77 ± 0.81 µm (ASP-I), 7.92 ± 2.34 µm (GII-3) and 5.24 ± 2.61 µm (ASP-I^{MreB5}) (Figure 2E), demonstrating that ASP-I cells, in the absence of MreB5, grew to shorter lengths compared to GII-3 and ASP-I^{MreB5}.

It is noteworthy that none of the other four MreBs could compensate for the absence of MreB5 for retaining helicity and motility in ASP-I cells. This shows that at

least a few of the MreBs may not be redundant in function and demonstrates the plausible existence of 'division of labour' among the multiple MreB paralogs in *Spiroplasma*. Analysis of all *Spiroplasma* genomes in the database revealed that they encode a minimum of 5 and maximum of 8 paralogs of *mreB* gene (Figure 3A). Based on the phylogenetic tree which showed 5 major MreB clusters (Figure 3A), we classified the MreBs per species into MreB1 – MreB5 (Table S1). The different paralogs of MreBs in each organism share pairwise average sequence identities in the range of 33 – 74 % (Figure 3B; Table S1), many of which are as divergent as MreB sequences from phylogenetically distant bacteria. An equivalent of MreB1 is absent in some of the species, and a few, including *S. citri* [11], have a duplicated MreB4 instead of MreB1 (M4* and M1/M4 clusters in Figure 3A; Table S1). We observed that Spiroplasmas possessing > 5 *mreB*s have duplicated or triplicated copies of either *mreB1, mreB4* or *mreB5* or combinations thereof (Figure 3C, Table S1). Despite an evolutionary pressure for a minimum genome, all *Spiroplasma* species maintain at least 4 different MreB types according to the above phylogenetic classification (Table S1). This is again suggestive of the requirement of multiple MreBs with distinct properties and functions.

In cell-walled bacteria, the proteins MreC, MreD (expressed as the *mreBCD* operon including MreB) and RodZ are essential for communication with the cell wall synthesis machinery during rod shape determination [21–24]. In the absence of cell wall in *Spiroplasma*, an alternative protein that moulds cell shape could be functional equivalents of MreC, MreD and RodZ. BLAST searches [25] using MreC, MreD and RodZ as queries against genomes of 26 species of *Spiroplasma* did not yield any hits. Analysis of neighboring genes of MreBs in *Spiroplasma* genomes revealed that there are no conserved neighbouring genes for *mreBs* across Spiroplasmas (Figure

3C). Further, investigation of the DNA sequences upstream of *mreB*s suggested that each *mreB* has its own promoter sequence (Figure 3D). These findings indicate that each MreB might be expressed independently and at different levels.

To understand the structural features of MreB from a cell wall-deficient bacteria, we determined the crystal structure of *Spiroplasma citri* MreB5 (a construct with a C-terminal hexahistidine tag denoted as MreB5-His_6; PDB ID: 7BVY; Figure 4A; Table S2). The crystal packing showed a single protofilament interface for MreB5-His_6, conserved among other structurally characterized MreBs from cell-walled organisms (eg. PDB ID: 1JCE of *Thermatoga maritima* MreB). Electron microscopy observations suggest that MreB5-His_6 forms antiparallel double protofilaments, a characteristic of MreBs [26,27] (Figure 4B, C). A double protofilament structure generated by superposition of MreB5 monomers on *Caulobacter crescentus* MreB (PDB ID: 4CZE) (Figure 4C) clearly shows that the projection in the 2D class averages corresponds to the antiparallel double protofilament organization.

Earlier reports suggest that fibril and MreB filaments are present near the cell membrane [15,16]. Also, in *C. crescentus* and *H. pylori*, MreB functions along with constitutive protein filaments such as crescentin and Ccm proteins for generating curved shapes [28–30]. We hypothesized that MreB5 should bind to the membrane and interact with fibril, a constitutive filament in *Spiroplasma*, for facilitating helical shape and motility. We therefore performed *in vitro* sedimentation assays to verify if MreB5-His_6 and fibril interact with each other. Our sedimentation assays showed that MreB5-His_6 does not pellet down whereas fibril is obtained in the pellet upon spinning at high speed (159,000 xg) (Figure 4D). However, in the presence of fibril, a fraction of MreB5-His_6 is also obtained in the pellet (Figure 4D, E). A control

experiment with hexahistidine-tagged mCherry instead of MreB5-His_6 did not co-pellet with fibril (Figure S2B). Hence, we concluded that MreB5-His_6 interacts with fibril. Further, when mixed with liposomes of composition mimicking *Spiroplasma* membrane and spun at high speeds (100,000 xg), MreB5-His_6 co-sedimented in the pellet fraction along with the liposomes indicating that it is capable of binding to the membrane (Figure 4F, G). A control experiment with RNaseA, a protein without lipid-binding properties, did not co-sediment with liposomes (Figure S2C). Hence, we speculate that MreB5 contributes to the cytoskeletal ribbon assembly in *Spiroplasma* by interacting with both fibril and the membrane.

A unique feature of *Spiroplasma* is the change in handedness of the cell body during motility. A bacterial flagellum achieves different helical conformations by varying lengths of constituent protofilaments [31]. An analogous model based on differential length changes of fibril filaments, required for generation of helicity and change in handedness, has been proposed for *Spiroplasma* [15,32,33]. Our study shows that MreB5 is an essential component for driving the proposed length changes. Since our results show that MreB5 interacts with the membrane lipids and fibril filaments, it is possible that MreB5 and fibril work in conjunction for a rod-shape to a helix transition. It is currently unknown if MreB5 contributes to the differential length changes of the filaments by driving conformational changes or promoting sliding between fibril filaments. Another possibility is that MreB5 undergoes conformational transitions followed by polymerization or de-polymerization, leading to length changes in itself.

Although helical shape seems to be one of the pre-requisites for kinking motility of *Spiroplasma*, helical shape does not ensure cell motility, for instance, the *scm1* mutant of *S. citri* was helical but non-motile [19]. The loss of helicity in late

exponential phase observed in both the helical strains, GII-3 and ASP-I^{MreB5} (Figure 2D), is presumably due to the dissipation of transmembrane potential [34]. Localization of MreB is also dependent on the membrane potential [35]. Inhibitors of rotary motors such as CCCP or DCCD, reportedly affect kinking motility [36,37]. The loss of helicity in the late exponential phase emphasizes that factors such as pH might contribute to maintain helicity. This further implies that components other than MreB5 and fibril are required for *Spiroplasma* helicity and motility.

MreB plays a role in DNA segregation [38,39], cell length regulation [38] and in *Myxococcus xanthus* motility [40], in addition to morphogenesis of cell-walled bacteria. *Bacillus subtilis* possesses three paralogs of MreB namely MreB, Mbl and MreBH. Each MreB paralog has been shown to polymerize independently, but their co-localizing assemblies are necessary for rod-shape in *B. subtilis* [41,42]. As demonstrated by our dissection of the role of MreB5 using the *S. citri* ASP-I strain, it will be exciting to investigate the individual roles of MreBs 1, 2, 3 and 4. The elongated, but shorter cells of ASP-I strain demonstrate that MreB1, 2, 3 or 4 or fibril might suffice to attain rod shape. The decreased length with no apparent increase in width of ASP-I cells (Figure 1E) or change in growth rate (inferred based on colony size) indicate that there may be additional mechanisms to maintain the cell width for a growing cell volume. One such mechanism is the Y-shaped division observed in *Spiroplasma* species [43], which might explain the instances of branched cells in ASP-I. MreB5 could regulate cell length through regulation of cell division events. Suppression of a cross-sectional division by a functional MreB5 could lead to longer cells while trigger of Y-shaped division in the absence of MreB5 maintains width.

We have experimentally demonstrated the requirement of MreB5 for maintaining cell length, helical shape and motility of a cell wall deficient bacterium, *S.*

citri. Thus, MreB5 serves as a bona fide cytoskeletal protein for shaping the cell. *Spiroplasma* MreBs perform their function independent of the cell wall synthesis machinery. The conserved structural features of MreB5 filaments compared to MreBs from cell-walled bacteria indicate that the fundamental mechanism of MreB to sculpt the cell might remain conserved across cell-walled and cell wall-deficient organisms. Thus cell wall-less organisms, such as the helical Spiroplasmas, provide us with multi-pronged approaches to study basic principles of cell shape determination.

Acknowledgments

Work in the lab of PG is supported by funds from Department of Science and technology (DST) INSPIRE Faculty Fellowship (IFA12/LSBM-52), Innovative Young Biotechnologist Award (BT/07/IYBA/2013), Department of Biotechnology Membrane Structural Biology Programme Grant (BT/PR28833/BRB/10/1705/2018) and IISER Pune. Common facilities at IISER Pune, the proteome and genome-transcriptome platforms of University of Bordeaux, France are acknowledged. We thank Pascal Sirand-Pugnet and Vincent Baby at INRAE, Bordeaux, France and Charlotte Mouden at the Genome Transcriptome facility (PGTB), Bordeaux, France for their help in handling genomic data. Help received from K.R. Vinothkumar (NCBS, Bangalore, India) and Mamta Bangera (InStem, Bangalore, India), Piotr Szwedziak and Martin Pilhofer (ETH, Zurich) and Armel Bezault (IECB, Bordeaux), for processing of electron microscopy samples at National Electron Cryomicroscopy Facility, Bangalore Life Sciences Cluster, India; ScopeM, ETH, Zurich; and IECB, Bordeaux respectively and access to the facilities is acknowledged. We thank synchrotron facilities EMBL-ESRF and DBT India for facilitating data collection at ID29, ESRF; and beamline scientists at I03 and I04 (MX14198, MX15369, MX16452,

and MX17251) at the Diamond Light Source, UK. We thank Dr. Thomas Pucadyil, IISER, Pune, India for the hexahistidine-tagged mCherry construct. We also thank funding agencies [SH: EMBO (STF 7225), CEFIPRA (RCF 2017/895), IISER Pune, Infosys foundation (IISER-P/InfyFnd/Trv/1); VP: IISER Pune, Infosys foundation (IISER-P/InfyFnd/Trv/174); and MB: IISER Pune].

Author contributions

SH designed, conceptualised, performed all experiments other than mentioned below, carried out data and sequence analyses and wrote the manuscript; SD performed and supervised the *Spiroplasma* molecular biology experiments; VP determined the crystal structure and performed electron microscopy experiments of MreB5, designed and performed liposome binding assays; MB assisted in representation of sequence analysis data, gene sequencing of *fibril* and *mreBs* of the two strains and in cloning of the complementation construct; LB designed, performed and supervised *Spiroplasma* genetics, biochemistry and microscopy experiments; PG designed, conceptualised and supervised *in vitro* experiments and sequence and structure analyses and wrote the manuscript. All authors reviewed and provided inputs for the manuscript.

Declaration of interests

The authors declare no competing interests.

Figure legends

Figure 1. Comparative characterization of *S. citri* GII-3 and ASP-I cells.

A. Light microscopy images of colonies of *S. citri* GII-3 cells (green box) and *S. citri* ASP-I cells (purple box). Within each box, the images on the left and right show unstained colonies and colonies stained with Dienes' stain, respectively. Red arrows point to diffused colonies. Scale bar represents 100 µm. **B.** Transmission electron microscopy (TEM) images showing morphology of *S. citri* GII-3 (wildtype; left) and ASP-I cells (right). The cell contour (L1) is marked in blue and the shortest distance between two points along its length (L2) is marked in red. Scale bar represents 0.5 µm. '*' symbols highlight branching points in cells, while '#' symbols mark a bulged tip. **C.** Distribution of ratios of cell length to the shortest distance between two points along its length (L1/L2) for *S. citri* GII-3 (green; n = 94) and *S. citri* ASP-I (purple; n = 94) cells. Each data point represents a cell. Mean and standard deviation is shown with long and short black lines respectively (unpaired t-test, *** $p \leq 0.001$). **D.** Number of crossovers of each cell per µm of L2 for *S. citri* GII-3 (green; n = 94) and *S. citri* ASP-I (purple; n = 94) cells is plotted. Each data point represents a cell. Mean and standard deviation is shown with long and short black lines respectively (unpaired t-test, *** $p \leq 0.001$). **E.** Cell width measurements for *S. citri* GII-3 (green; n = 94) and ASP-I (purple; n = 108). Each data point represents a cell. Mean and standard deviation is shown with long and short black lines respectively (unpaired t-test, *** $p \leq 0.001$). **F.** DNA sequences of region in *mreB5* gene from *S. citri* GII-3 (top) and *S. citri* ASP-I (bottom). Amino acids coded by respective codons are written above (*S. citri* GII-3) and below (*S. citri* ASP-I) the DNA sequences. Highlighted in grey background is the codon in *S. citri* ASP-I with point mutation (refer Figure S1 for chromatogram) and the corresponding codon in *S. citri* GII-3. Numbers in superscript indicate the position of the nucleotide/amino acid from the start codon/first amino acid in the sequence. **G.** Plot showing relative abundance (in log scale) of the 5

MreBs from *S. citri* GII-3 (green) and ASP-I (purple) cells in the membrane and cytosolic fractions.

Figure 2. MreB5 confers helicity and motility in *S. citri* ASP-I cells.

A. Light microscopy images of colonies of *S. citri* ASP-I cells transformed with empty pSD4 vector (*S. citri* ASP-I^{pSD4}; top) and *mreB5* cloned in pSD4 (*S. citri* ASP-I^{MreB5}; bottom). Within each box, the images on the left and right show unstained colonies and colonies stained with Dienes' stain, respectively. Red arrows point to diffused colonies. **B.** Snapshots from videos (see also Videos S1- S3) of *S. citri* strains GII-3 (left, green box), ASP-I (middle, purple box), and ASP-I^{MreB5} (right, orange box) showing cell morphologies at periodic time points. Time range lies between the values mentioned on first and last frames for a given cell and with equal time intervals between subsequent frames. Coloured arrows point to the kinks in the cell body. Scale bar represents 3 µm. **C.** Distribution of velocities of *S. citri* strains GII-3 (green, n = 32), ASP-I (purple, n = 39) and ASP-I^{MreB5} (orange, n = 40). Each data point represents the velocity of a cell. Mean and standard deviation is shown with long and short black lines respectively (unpaired t-test, *** $p \leq 0.001$; ** $p \leq 0.01$; ns (non-significant) $p > 0.05$). **D.** Distribution of ratios of cell length to the shortest distance between two points along the cell length (L1/L2) for *S. citri* GII-3 (green), ASP-I (purple) and ASP-I^{MreB5} (orange) cells. The data in exponential and late exponential phases of cell growth are represented by solid circles and crosses respectively (n = 50 each for all cases). Mean and standard deviation is shown with long and short black lines respectively (unpaired t-test, *** $p<0.0001$; * $p \leq 0.05$; ns (non-significant) $p > 0.05$). **E.** Distribution of cell lengths of *S. citri* GII-3 (green), ASP-I (purple), and ASP-I^{MreB5} (orange) in exponential (solid circles) and late exponential

(cross) phases of growth. Mean and standard deviation is shown with long and short black lines respectively (unpaired t-test, *** $p<0.0001$; * $p \leq 0.05$).

See also Figure S2 for PCR tests for confirmation of strains and Videos S1 – S3.

Figure 3. Classification of *Spiroplasma mreBs*

A. Rooted phylogenetic tree [44,45] showing distribution and classification of MreBs from 26 species (27 strains including two strains of *S. citri* ScR8A2 and ScGII3 are included) of *Spiroplasma* into 5 clusters. Sequences of MreBs and FtsA from *E. coli, B. subtilis, C. botulinum* and *C. crescentus* as well as Mbl and MreBH from *B. subtilis* were also included in the tree. MreBs are color coded according to the clusters [MreB1 (M1, orange), MreB2 (M2, green), MreB3 (M3, purple), MreB4 (M4, dark pink), duplicated MreB4 (M4*, light pink), MreB1/MreB4 (M1/M4; red), MreB5 (M5, dark cyan), MreBs, Mbl and MreBH from cell walled bacteria (grey), FtsA from cell walled bacteria (black)]. M1/M4 is a branch in the phylogenetic tree which has not been classified into either M1 or M4 and hence mentioned as M1/M4. **B.** Percentage sequence identity matrix among *Spiroplasma* MreBs belonging to 5 clusters [46]. The percentage identity among *S. citri* GII-3 MreBs is shown in black color (squares to the right of the diagonal) while average percentage identities among MreBs belonging to the 5 different clusters of each species (averaged across 26 species of *Spiroplasma* according to the classification in Table S1) are shown in grey color (squares to the left of the diagonal). Sequences belonging to the class M1/M4 were excluded from the averaging, while M4* (duplicated M4) were considered as M4 in the pairwise matrix. **C.** Schematic representation of genes neighboring *Spiroplasma mreBs*. Neighbors (+3 and -3 positions) of *mreB* genes from *Spiroplasma* species have been aligned and depicted as arrows. The arrows with black borders represent

MreBs (color coded as in Figure 3A), while arrows with grey borders represent genes neighboring *mreBs* and colour coded according to their annotation (shown by the colour key in the right box). The direction of the arrows indicates gene orientation 5' → 3'. Asterisk and white arrow with black border represents a *mreB* pseudogene that translates into a truncated MreB. **D.** Weblogos of consensus sequences predicted to be -35 and -10 sequences for the 5 clusters of *mreBs* across 26 *Spiroplasma* species [47]. These sequences can act as promoter elements and facilitate expression of each *mreB* independent of other *mreBs* in the genome.

See Table S1 for further details of MreB classification.

Figure 4. MreB5-His$_6$ possesses anti-parallel double protofilament assembly *in vitro* and interacts with fibril and liposomes.

A. Crystal structure of *S. citri* MreB5 (with a C-terminal hexahistidine tag; MreB5-His$_6$; PDB ID: 7BVY; see Table S2 for data collection and refinement statistics) shows a single protofilament organization according to crystal packing. Three adjacent monomers are shown and the subdomains are color coded and labelled as 1A, 2A, 1B and 2B. The black arrow corresponds to a direction of the protofilament with subdomains 1A and 2A at the base (barbed end according to actin nomenclature). **B.** Electron cryomicroscopy images of MreB5-His$_6$ filaments *in vitro*. Insets highlight the double protofilaments in a zoomed section of the image (bottom left) and show the top four 2D class averages of segment of filaments (bottom right). **C.** A view of the double protofilament structure of MreB5-His$_6$, modeled based on *Caulobacter crescentus* MreB (PDB ID 4CZE), matches with the projection view of the 2D class averages in panel (B). The subdomains are color-coded as in panel (A). The view corresponds to an orientation with 1A and 1B sub-domains behind the

plane of 2A and 2B sub-domains. The orientation of the protofilaments is highlighted by the black arrows, marked according to the convention in panel (A). **D.** A representative 12 % SDS-PAGE gel showing sedimentation assays of untagged fibril, MreB5-His_6 and MreB5-His_6 in presence of fibril (untagged). I, P and S respectively represent input, pellet and supernatant fractions upon sedimentation at 159,000 xg. Red and blue '*' symbols show the full length bands of fibril and MreB5, respectively, while the lower bands are the impurity or degradation bands obtained during fibril purification. **E.** A plot showing relative mean intensities (expressed in percentage) of bands corresponding to MreB5-His_6 position (marked by blue * and region enclosed by dashed blue box) in the SDS-PAGE gels from 3 independent experiments, as described in panel (D). The relative intensities of pellet (or supernatant) fractions at the position corresponding to MreB5-His_6 band were calculated as intensity of pellet (or supernatant) divided by sum of the two intensities and represented in the graph as a percentage. Pel and Sup represents the pellet and supernatant fractions, respectively, upon spinning at 159,000 xg. **F.** A representative 12 % SDS-PAGE gel showing sedimentation of MreB5-His_6 upon adding increasing concentrations of liposomes. P and S respectively represent pellet and supernatant fractions upon sedimentation at 100,000 xg. Lanes 2 and 3 are repeats of the samples in lanes 4 and 5 along with a protein molecular weight marker (note that the band intensities differ for the same concentrations due to use of a 10-well gel). **G.** A plot showing relative mean intensities (expressed in percentage) of bands corresponding to MreB5-His_6 position in the SDS-PAGE gels from 3 independent experiments, as shown in panel (F). The relative intensities of pellet (or supernatant) fractions at the position corresponding to MreB5-His_6 band were calculated as intensity of pellet (or supernatant) at the position corresponding to MreB5-His_6 band

divided by sum of the two intensities and represented in the graph as a percentage. See Figure S2 for control experiments for sedimentation and liposome binding assays, and Table S3 for the list of strains and plasmids used.

STAR Methods

RESOURCE AVAILABILITY

LEAD CONTACT

Further information and requests for resources and reagents should be directed to and fulfilled by the Lead Contact, Pananghat Gayathri (gayathri@iiserpune.ac.in).

MATERIALS AVAILABILITY

Spiroplasma strains and the plasmids generated in the study are available with Laure Béven (laure.beven@inrae.fr), while the plasmids for MreB5-His_6 and fibril proteins in *E. coli* are available with Pananghat Gayathri (gayathri@iiserpune.ac.in).

DATA AND CODE AVAILABILITY

The whole genome sequencing read of *S. citri* ASP-I is deposited in the Sequence Read Archive at NCBI, under accession number (Bioproject PRJNA635252). The accession number for the crystal structure of MreB5-His_6 complexed with AMPPNP reported in this paper is PDB ID: 7BVY.

EXPERIMENTAL MODEL AND SUBJECT DETAILS

Cultures

S. citri GII-3 [48] and *S. citri* ASP-I [18] cultures available in the lab of Dr. Laure Béven were used in the present study. All *Spiroplasma* cells in the present study were grown in modified SP4 medium [Composition per 300 mL of media: A)

Components to be autoclaved: 1 g Mycoplasma base broth, 1.6 g peptone, 3 g tryptone, 1.2 mL phenol red (9 mg/mL 1M NaOH), adjust pH to 7.6, make up the volume to 205 mL with MilliQ grade water. B) Components to be filter sterilized and added to autoclaved components: 50 mL heat-inactivated foetal calf serum, 15 mL CMRL 1066 (10X), 25.5 mL Yeastolate (stock concentration 4 % w/v), 3 mL D-glucose (50 % w/v) and 1.5 mL Penicillin G (stock concentration 200,000 U/mL)] [49].

E. coli cell strains used in this study for cloning, Stellar™ (Takara Bio) electro-competent *E. coli*, and for protein expression *E. coli* BL21 (AI), were grown in LB (Luria Bertani) broth supplemented with ampicillin (final concentration 100 µg/mL) at 37 °C.

METHOD DETAILS

Electron microscopy imaging of *Spiroplasma* and cell length analysis

Growing cells (80 µL) of *S. citri* GII-3 or ASP-I were mixed with 20 µL Protein A-conjugated colloidal gold nanoparticles (10 nm, Cytodiagnostics). 5 µL of this mixture was applied to a glow-discharged EM grid (R2/2, 200 mesh, copper, Quantifoil) and left at room temperature (25 °C) for 60 seconds. The grids were transferred to Vitrobot™ (Marc IV, FEI; chamber at 32 °C with 95 % humidity) and excess media absorbed by back-blotting manually using a blotting paper (TED PELLA, INC.). The grid was plunge frozen in a mixture of ethane and propane (37 % : 63 % v/v) and then transferred to labelled grid storage box. Boxes containing frozen grids were stored in liquid nitrogen for at least 24 hours before imaging. The samples were observed and images acquired using Titan Krios (300 KeV; FEI) electron microscope with K2 Summit direct electron detector and Quantum LS imaging filter.

ImageJ 1.52p (USA) [50] was used for the measurement of cell contour (L1) and the shortest distance between two points along cell body length (L2) from electron microscopy images. The cell length refers to the contour length L1 at all instances in the text, while cell width is the extent of cells along a cross section approximately perpendicular to the cell contour line. The data is expressed as the mean ± standard deviation (SD). Statistical significance was estimated by the unpaired t test, two tailed. GraphPad Prism 5.00 for Windows (GraphPad Software, San Diego California USA, www.graphpad.com) was used for statistical analysis of the data and plotting the graphs.

DNA isolation and sequencing

With 100 ng of *S. citri* GII-3 and ASP-I genomic DNA as template, the 5 *mreB* and *fibril* genes were PCR amplified using the flanking primers given in Table S3, followed by gene sequencing.

Whole genome sequencing

Whole genome sequencing of *S. citri* ASP-I was performed at the Genome Transcriptome facility of Bordeaux (https://pgtb.cgfb.u-bordeaux.fr/) using a combination of Oxford Nanopore (GridION sequencer) and paired-end 250 bp Illumina (MiSeq sequencer) reads. The genome was assembled into 4 main contigs using both short and long reads and the Unicycler v0.4.6 pipeline (PMID: 28594827). One contig of 7999 bp corresponded to the previously described plasmid pSciA (GenBank accession AJ966734.1). The three chromosomal contigs came up to a total of 1493377 bp.

Protein extraction and proteomic analysis

Spiroplasma proteins were extracted, using the protocol as reported earlier [51]. Briefly, a 50 mL culture pellet of *Spiroplasma* cells (ASP-I and GII-3) was re-suspended into 1 mL Tris-buffered saline [TBS; 10 mM Tris-HCl (pH 7.4), 150 mM NaCl] and lysed by sonication. 100 µL extraction buffer [10 mM Tris (pH 7.4), 154 mM NaCl] and 100 µL Triton X-114 (10 % w/v) were added to 800 µL lysate on ice, to facilitate extraction of membrane proteins by Triton X-114. This was followed by separation of the mixture into insoluble fraction, Triton X-114 soluble fraction and supernatant, as described in the reference. Fractions containing total proteins, aqueous soluble proteins and Triton X-114 solubilized proteins were checked on a 12 % SDS-PAGE gel. Proteins were identified by peptide mass fingerprint and tandem-mass spectrometry (MS/MS) sequencing from protease-digested protein at the Proteome Platform, Functional Genomic Center of Bordeaux, University of Bordeaux as follows.

Sample preparation and protein digestion

Protein samples were solubilized in Laemmli buffer [2X; SDS (4 % w/v), Bromophenol blue (0.2 % w/v), glycerol (20 % v/v), DTT (200 mM), and 100 mM Tris-HCl, pH 6.8] and 5 µg were deposited onto preparative SDS-PAGE for concentration and cleaning purpose. Separation was stopped once proteins entered the resolving gel. After colloidal blue staining, each lane was cut in 1 mm x 1 mm gel pieces. Gel pieces were de-stained in 50 % acetonitrile (ACN) containing 25 mM ammonium bicarbonate (ABC), rinsed twice in ultrapure water and shrunk in ACN for 10 min. After ACN removal, gel pieces were dried at room temperature, covered with the trypsin solution (10 ng/µL in 50 mM ABC), rehydrated at 4 °C for 10 min, and finally incubated overnight at 37 °C. Spots were then incubated for 15 min in 50 mM ABC at room temperature with rotary shaking. The supernatant was collected, and

an H_2O/ACN/formic acid (47.5 : 47.5 : 5) extraction solution was added onto gel slices for 15 min. The extraction step was repeated twice. Supernatants were pooled and dried in a vacuum centrifuge. Digests were finally solubilized in 0.1 % formic acid.

nLC-MS/MS analysis

Peptide mixture was analyzed on a Ultimate 3000 nanoLC system (Dionex, Amsterdam, The Netherlands) coupled to a Electrospray Orbitrap Fusion™ Lumos™ Tribrid™ Mass Spectrometer (Thermo Fisher Scientific, San Jose, CA). 10 µL of peptide digests were loaded onto a 300 µm (inner diameter) x 5 mm C18 PepMapTM trap column (LC Packings) at a flow rate of 10 µL/min. The peptides were eluted from the trap column onto an analytical 75 mm (inner diameter) x 50 cm C18 Pep-Map column (LC Packings) with a 4 – 40 % linear gradient of solvent B in 45 min (solvent A was 0.1 % formic acid and solvent B was 0.1 % formic acid in 80 % ACN). The separation flow rate was set to 300 nL/min. The mass spectrometer operated in positive ion mode at a 1.9 kV needle voltage. Data were acquired using Xcalibur 4.1 software in a data-dependent mode. MS scans (m/z 375-1500) were recorded at a resolution of R = 120 000 (@ m/z 200) and an AGC target of 4 x 105 ions collected within 50 ms. Dynamic exclusion was set to 60 s and top speed fragmentation in Higher-energy collisional dissociation (HCD) mode was performed over a 3 s cycle. MS/MS scans with a target value of 3 x 103 ions were collected in ion trap with a maximum fill time of 300 ms. Additionally, only + 2 to + 7 charged ions were selected for fragmentation. Others settings were as follows: no sheath, nor auxiliary gas flow, heated capillary temperature, 275 °C; normalized HCD collision energy of 30 % and an isolation width of 1.6 m/z. Monoisotopic precursor selection (MIPS) was set to Peptide and an intensity threshold was set to 5 x 10^3.

Database search and results processing

Data were searched by SEQUEST through Proteome Discoverer 2.3 (Thermo Fisher Scientific Inc.) against homemade protein databases consisting of products of *S. citri* ASP-I and GII-3 CDS (Chromatography Data System). Spectra from peptides higher than 5000 dalton (Da) or lower than 350 Da were rejected. The search parameters were as follows: mass accuracy of the monoisotopic peptide precursor and peptide fragments was set to 10 parts per million (ppm) and 0.6 Da respectively. Only b- and y-ions were considered for mass calculation. Oxidation of methionines (+ 16 Da) and protein N-terminal modifications (Acetylation + 42 Da) were considered as variable modifications and carbamidomethylation of cysteines (+ 57 Da) as fixed modifications. Two missed trypsin cleavages were allowed. Peptide validation was performed using Percolator algorithm [52] and only “high confidence” peptides were retained corresponding to a 1 % false-positive rate at peptide level. Peaks were detected and integrated using the Minora algorithm embedded in Proteome Discoverer. Proteins were quantified based on unique peptides intensities. Normalization was performed based on total protein amount.

Cloning, transformation and colony characteristics

The *ef-tu* (*tuf*) promoter region from pSTP1 vector [53] was amplified using primers P1 and P2 (Table S3). The *mreB5* gene was amplified from genomic DNA of *S. citri* GII-3 cells using primers P3 and P4. The amplified products of these two PCRs were purified using a PCR clean-up kit (Qiagen) and eluted in 30 µL MilliQ water separately. An overlap-extension PCR was set up using the purified PCR products to obtain the *tuf* promoter-*mreB5* DNA fragment. The product DNA was extracted from the gel using a gel extraction kit (Qiagen) and re-amplified using end primers. The

amplified product was cleaned up, digested with restriction enzyme EcoRI and cloned into the pSD4 vector [54] by restriction digestion-ligation method. The ligation reaction was transformed into Stellar™ (Takara Bio) electro-competent *E. coli* cells by electroporation. The obtained transformants were grown in LB (Luria Bertani) broth supplemented with ampicillin (final concentration 100 µg/mL) and plasmid extracted using a QIAprep miniprep kit (Qiagen). DNA sequence inserted into the plasmid was sequenced using M13 forward and EV13 primers (Table S4) to confirm the sequence.

Transformation

In two different reactions, the confirmed clone and empty pSD4 vector (control) was transformed into growing *S. citri* ASP-I cells using the previously described protocol [55]. 500 ng of *mreB5* clone or empty pSD4 vector was transformed into *S. citri* ASP-I cells by electroporation using MicroPulser Electroporator (Bio-Rad) and following parameters- 2500 V voltage, 3 µF capacitance, 1000 Ω resistance, and spread on SP4 agar plates supplemented with tetracycline (final concentration of 2 µg/mL). The plates were incubated at 32 °C until the development of colonies. Appearance of colonies was monitored by observation of plates, using a binocular loupe until colonies were visible.

Diene's staining

Colonies were stained with Dienes's stain using the method described [20]. Spiroplasmas grown in liquid SP4 were diluted with fresh SP4 to a concentration of about 10^3 cells/mL. The diluted suspensions were plated on SP4 containing 1 % Difco™ Agar Noble (Becton, Dickinson and Company, USA) in petri dishes (5 cm

diameter) and incubated at 32 °C for 14 days. Dienes' stain was prepared by dissolving 2.5 g methylene blue, 10 g maltose, 1.25 g azure II and 0.25 g sodium carbonate in 100 mL ultrapure water and filtered through Whatman filter paper No.1. The colonies were stained in Dienes' stain diluted to 3 % (v/v) (5 mL/Petri dish) for 5 min. The stained colonies were then extensively rinsed in distilled water, and examined using a microscope Nikon SMZ1270, equipped with the camera Nikon DS-Fi2. Images were acquired using the software NIS-Elements D.

PCR-based confirmatory tests for clones

Total DNA (including genomic DNA and plasmids) was extracted from *S. citri* GII-3 and ASP-I cells transformed with either *mreB5* gene cloned in pSD4 vector (*S. citri* ASP-I^{pSD4}) or empty pSD4 vector (*S. citri* ASP-I^{MreB5}) using the Wizard® Genomic DNA purification kit (Promega). Three sets of PCRs were performed to confirm that the transformants obtained by electroporation of *S. citri* ASP-I cells with the pSD4 vector containing *tuf* promoter-*mreB5* gene were indeed transformants. The first PCR was performed using *sr14* and *sr16* primers [56] (Table S3) as positive control for amplifying a fragment of the *spirallin* gene. The second PCR was carried out using *tet1* and *tet2* primers [57] (Table S3) to confirm the presence of the tetracycline-resistance gene carried on the pSD4 vector. The third PCR was performed using *Scarp* 235 primers [58] (Table S3) to check for the presence of genes coding for *S. citri* adhesion-related proteins (SCARPs) carried on pSci vectors that are present in *S. citri* GII-3 cells but absent in *S. citri* ASP-I^{pSD4} and *S. citri* ASP-I^{MreB5} cells. The PCRs against total DNA of *S. citri* GII-3 cells and *S. citri* ASP-I^{pSD4} were set up as controls. All the PCR products were migrated on agarose gels (2 % w/v) and visualized by ethidium bromide staining (Figure S2A).

Dark-field microscopy, cell length measurements and velocity calculations

The morphology of exponentially growing GII-3, ASP-I, ASP-I^{pSD4} and ASP-I^{MreB5} cells of *S. citri* in modified SP4 media was observed using an Eclipse Ni (Nikon) microscope working in reflection and equipped with a dark field condenser. The Nikon oil immersion microscope objective was a 60X with a numerical aperture (N. A.) of 0.80. Pictures were taken with a camera Nikon Digital Sight DS-Qi1Mc (1280 × 1024 pixels). Motility was favoured by increasing the viscosity of the medium following the protocol described in [59]: during the exponential growth phase of the bacteria, one volume of the culture was diluted with one volume of methyl cellulose dissolved in modified SP4. Here, 1 % (w/v) methyl cellulose [from Sigma (M7027), Molecular weight 14000 g/mol] was used to adjust the viscosity of the solutions. Bacterial solutions were prepared between two sealed microscope slides, with a liquid thickness of 15 µm. Videos were recorded at a frame rate of 10 frames per second (fps) using the software NIS-Elements Br (Nikon). *Spiroplasma* cell velocities were estimated from videos using the 'Manual Tracking' plugin in ImageJ [50]. Similarly, cell lengths and widths were measured from images using ImageJ. The data is expressed as the mean ± standard deviation (SD). Statistical significance was estimated by the unpaired t test, two tailed. GraphPad Prism 5.00 for Windows (GraphPad Software, San Diego California USA, www.graphpad.com) was used for statistical analysis of the data and plotting the graphs.

MreB sequences analysis and classification

mreB gene and protein sequences were obtained from NCBI (https://www.ncbi.nlm.nih.gov/). The genes from each species were labelled in order of their appearance in the genome with respect to *dnaA*, with the closest *mreB* at the

3' of *dnaA* being assigned number 1. All the MreB protein sequences were aligned using Clustal Omega [46] with default settings. A phylogenetic tree was prepared using all the aligned MreB sequences with the help of NGPhylogeny [44] using default settings and visualized using IToL [45].

Analysis of neighborhood genes

To analyze the neighboring genes of *mreBs*, 3 genes each at the 5' and 3' ends of respective *mreBs* in the genome were considered. The genes were labelled in sequential order such that the gene preceding (at the 5' end of) *mreB* was labelled as -1 position and the gene at the 3' end of *mreB* was assigned +1 position and so on. In order to check if the hypothetical proteins at a given position are identical, amino acid sequences of hypothetical proteins at that position were aligned using Clustal Omega [46] and protein conservation checked. To check if the MreC, MreD and RodA homologs are present in *Spiroplasma* species, sequence of corresponding genes and proteins from *E. coli* K-12 (MG1655) was used. The sequence was provided as a query for BLAST [25] against each of the 26 species of *Spiroplasma* using default parameters.

Identification of *mreB* promoter regions

Nucleotide sequence corresponding to 100 basepairs (bp) region upstream (before the 5' end) of each *mreB* gene of *Spiroplasma* species under consideration was obtained from NCBI. The -35 and -10 elements from 100 bp regions of all *mreBs* were identified using BPROM software [47]. The identified -35 and -10 sequences for all MreBs from a cluster (grouped on the basis of phylogenetic tree) across species were used for generating a Weblogo using WebLogo 3 [60].

Fibril expression and purification

The *fibril* gene from *S. citri* (DSMZ 21846) genomic DNA was cloned into the pHIS17 vector (refer Addgene plasmid # 78201 for plasmid backbone) [61]. The cloning and standardization of expression and purification is described in Harne, et al., (manuscript to be communicated). The protein was over-expressed using *E. coli* BL21 (AI) cells by growing the transformants in Luria Bertani (LB) broth supplemented with ampicillin (100 µg/mL final concentration) at 37 °C under shaking conditions until OD_{600} = 0.6. The cells were induced by addition of sterile L-arabinose at final concentration of 0.2 % (w/v) and were grown at 25 °C for 6 hours post-induction. The cells were harvested and lysed by sonication in 50 mM Tris pH 8.0. The lysate was spun at 30,000 xg to get rid of cell debris and other macromolecules as a pellet. The supernatant containing fibril was further spun at 159,000 xg, 4 °C for 30 minutes and fibril obtained in the pellet. The fibril containing pellet was re-suspended in 1 mL of buffer containing 10 mM Tris pH 8.0 and 10 mM EDTA and stirred at 4 °C overnight. The stirred fibril solution was loaded on top of a urografin (76 % w/v; Cadila healthcare Ltd, Kundaim, India) linear gradient. The gradient was prepared by layering equal volumes of 34 % [v/v in $T_{10}E_{10}$ (10 mM Tris pH 8.0, 10 mM EDTA) buffer] and 76 % urografin followed by overnight incubation at room temperature. The fibril-loaded gradient was spun at 159,000 xg/ 4 °C / 120 minutes and fractionated into 10 equal fractions and visualized on a 12 % SDS-PAGE gel. Fractions containing fibril were pooled and washed with 50 mM Tris (pH 7.6) by 2 cycles of pelleting and re-suspension to remove urografin. The pellet containing enriched fibril was re-suspended in minimum volume of reaction buffer [50 mM Tris (pH 8.0), 300 mM KCl and 2 mM $MgCl_2$].

MreB5-His_6 purification

The *S. citri* (DSMZ 21846) *mreB5* gene with a hexa-histidine tag was cloned into a pHIS17 vector [61] and over-expressed in *E. coli* BL21 (AI) cells. The standardization of purification conditions and buffer optimization are described in Pande, et al., (manuscript to be communicated). The cells were grown in LB broth at 37 °C until OD_{600} was 0.8-1.0. The culture was induced with L-arabinose at a final concentration of 0.05 % (w/v). Post-induction, the culture was grown at 20 °C for 12 hours. For large scale protein purification, 2 litres of cell pellet was thawed and cells were homogenized in lysis buffer (300 mM KCl, 50 mM Tris, pH 8.0 and 10 % glycerol) and lysed by sonication. The lysate was centrifuged at 44,082 xg for 45 mins at 4 °C. The supernatant was loaded on 5 mL Ni-NTA column (HisTrap, GE Healthcare) pre-equilibrated with buffer A (50 mM Tris pH 8.0, 300 mM KCl). Hexahistidine tag present in the C-terminus of protein facilitated binding to Ni-NTA column. Bound protein was eluted using a step gradient of 5 %, 10 %, 20 %, 50 % and 100 % of buffer B (50 mM Tris pH 8.0, 300 mM KCl and 500 mM Imidazole). Fractions containing purest protein were identified by visualization on 12 % SDS-PAGE gel, pooled and dialyzed against buffer containing 50 mM Tris pH 8.0, 300 mM KCl. Protein purification and dialysis was carried out at 4 °C. Purified protein was further concentrated using centricons with 10 kDa cutoff (Sartorius), flash frozen and stored in -80 °C until further use.

For sedimentation experiments to study interaction with fibril, MreB5-His_6 was expressed as described above. Purification was done using Ni-NTA His-bind Superflow resin (Sigma) on the bench using a syringe column, eluted with buffer B, fractions containing pure protein were pooled and concentrated using concentrators with 3 kDa cut-off. The imidazole was removed by cycles of dilution during the concentration step, resulting in a final buffer composition of 50 mM Tris pH 8.0, 300

mM KCl with negligible imidazole. The purified MreB5 was used for the sedimentation assays the same day.

mCherry expression and purification

mcherry gene with a hexahistidine tag at its 5' end, cloned in pET15b vector was obtained from Dr. Thomas Pucadyil, IISER, Pune, India. The clone was transformed into *E. coli* BL21 (AI) cells by heat shock method. Single colony was inoculated in 20 mL LB broth supplemented with ampicillin at final concentration of 100 µg/mL and incubated at 37 °C under shaking conditions for 12 hours. 5 mL of this culture was inoculated into 1 Litre LB broth (supplemented with ampicillin at final concentration of 100 µg/mL) and grown under shaking condition at 37 °C until OD_{600} reached 0.6. The cells were induced by addition of sterile L-arabinose at final concentration of 0.2 % (w/v) and further were grown at 25 °C for 6 hours post-induction. The cells were harvested and lysed by sonication in lysis buffer containing 50 mM Tris pH 8.0, 300 mM KCl and 10 % (v/v) glycerol. The lysate was spun at 159,000 xg to get rid of cell debris as a pellet. The supernatant containing mCherry was used for purification on bench using Ni-NTA His-bind Superflow resin (Sigma) in a syringe column and concentrated using the protocol same as that used for MreB5 purification for sedimentation assay (described above).

Sedimentation assay

Purified MreB5-His_6 was spun at 159,000 xg, 25 °C for 30 minutes to remove denatured and/or aggregated MreB5-His_6 as pellet. Protein in the supernatant was used for concentration estimation and sedimentation assay experiments. Similarly, enriched fibril was also spun under the same conditions to pellet down fibril filaments and then pellet re-suspended in reaction buffer. Since fibril was insoluble in the

buffer, its concentration was estimated by solubilizing small aliquot of fibril with addition of sodium dodecyl sulphate (SDS) at a final concentration of 1 % (w/v) and by measuring absorbance at 280 nm using NanoDrop (ThermoFisher Scientific).

Equimolar concentrations of purified MreB5-His_6 and enriched fibril were mixed in the reaction buffer [50 mM Tris (pH 8.0), 300 mM KCl and 2 mM $MgCl_2$]. As controls, reactions containing only MreB5-His_6 and only fibril samples were used. All the tubes containing reactions were incubated at 25 °C for 30 minutes and then spun at 159,000 xg/ 25 °C for 30 minutes. The supernatant was transferred to a new tube and the pellet was re-dissolved in reaction buffer with the final volume same as that of the initial reaction volume (typically 50 µL). Equal volumes of supernatant were mixed with 2X Laemmli buffer and visualized using 12 % SDS-PAGE gels.

The intensity of protein bands corresponding to the MreB5-His_6 band on SDS-PAGE gels was analyzed using ImageJ 1.52p (USA) [50]. To calculate the fractional intensity % of MreB in the pellet and supernatant, the intensities of the bands from pellet or supernatant samples were multiplied by 100 and divided by the sum of the intensities the bands in pellet and supernatant. The data in the graph is expressed as the mean ± standard deviation (SD).

As a negative control, the sedimentation experiment was repeated by using mCherry-His_6 instead of MreB5-His_6.

Liposome preparation

All the lipids used for liposome preparation were purchased from Avanti Polar Lipids, 1,2-dioleoyl-sn-glycero-3-phosphocholine (DOPC, 850375C), 1,2-dioleoyl-sn-glycero-3-phospho-(1′-rac-glycerol) (DOPG, 840475C), Brain SM (Sphingomyelin (Brain, Porcine), 860062C), *E. coli* Cardiolipin (841199C). To obtain a final working

concentration of the liposome for the assay to 2 mM, 0.28 mM of DOPC, 0.76 mM of DOPG, 0.66 mM of Brain SM and 0.30 mM of *E. coli* CL chloroform solutions were aliquoted in a clean test tube and dehydrated to remove the chloroform. The concentrations of these liposome were chosen based on the available molar ratio of membrane lipids found in *S. citri* [62]. For preparing the liposome, dried lipid mixtures were hydrated in buffer A (300 mM KCl, 50 mM Tris, pH 8.0) containing 1 mM $MgCl_2$ to a final concentration of 2 mM. This mixture was extruded through 100 nm polycarbonate membranes (Avanti Polar Lipids).

Liposome pelleting assay

Protein aliquot of MreB5-His_6 was spun at 100,000 xg for 25 mins at 4 °C. 2 µM of protein from the supernatant was added to the reaction mixture of 100 µL containing liposomes in buffer A (300 mM KCl, 50 mM Tris pH8.0) and 1 mM $MgCl_2$. The reaction was incubated at room temperature for 15 mins. Post incubation, the reaction was spun at 100,000 xg for 25 mins at 25 °C. The supernatant was carefully removed and the pellet was re-suspended in 50 µL of buffer A. Supernatant and pellet were mixed with 2X Laemmli buffer and equal amounts of the pellet and supernatant were loaded on 12 % SDS-PAGE gel. The intensity analysis of protein bands were performed on ImageJ 1.52n [50]. The fractional intensity % calculation was performed in the same way as described for sedimentation assay above. The data in the graph is expressed as the mean ± standard deviation (SD). RNaseA (Sigma-Aldrich) at equivalent concentrations was used instead of MreB5-His_6 in negative control experiments.

Crystallization and Structure determination of MreB5

About 960 conditions of commercially available screens (Molecular dimensions, Hampton Research) were screened, using drop sizes containing 100 nL of protein (4 mg/mL) and 100 nL of crystallization condition. Initial hits were seen for many of the conditions and were further optimized to get a well diffracting crystal. Diffraction quality crystals were obtained in the condition containing 4.1 mg/mL protein crystallized with 2 mM AMPPNP and 2 mM Mg^{2+} in a condition containing 0.15 M Na-K phosphate, 16 % PEG 3350, pH 7.8 by hanging drop method at 1:1 ratio. The crystal was frozen in 20 % glycerol cryo-protectant contained in the parent condition for diffraction. Data for the crystal was collected at ESRF. The crystal diffracted to 2.5 Å. Data reduction was performed using DIALS [63] and data scaling using AIMLESS [64] in the CCP4i2 [65] package. Molecular replacement was done using ScMreB5-ADP (PDB ID: 7BVZ) in PHASER [66] available in the CCP4 [67] package. Refinement was performed using the PHENIX package [68] and model building using Coot [69]. Data collection and refinement statistics are summarized in Table S3.

Electron cryomicroscopy and filament assembly model of MreB5

For visualizing filaments of MreB5-His_6 electron cryomicroscopy was performed. Quantifoil (Au 1.2/1.3) grids were used that were glow discharged for 90 sec. Protein samples were centrifuged at 100,000 xg for 25 mins at 4 °C. For protein polymerization, 50 µM of protein was incubated with 5 mM ATP and 5 mM $MgCl_2$ at 25 °C for 10-15 mins. The glow discharged grid was mounted on the VitrobotTM (Mark IV, FEI) , 3 µL of the sample was put on the grid and incubated for 5-10 sec before blotting for 3 sec followed by plunge freezing into liquid ethane for vitrification. For image acquisition, grids were mounted on Triton-Krios 300 KeV with Falcon-3 direct detector and images were acquired at a magnification of 59,000X. Images of

the filaments were observed using ImageJ 1.52n [70]. 2-D class averages were generated using default options in RELION software [71].

Double protofilament assembly of MreB5 was generated by superposing MreB5 coordinates sub-domainwise on the double protofilament assembly of CcMreB (PDB ID- 4CZJ) using Coot 0.8.9.1 [69]. Using UCSF Chimera version 1.13.1 [72] each subdomain of ScMreB5 was saved as separate PDB files. The subdomains, IA, IB, IIA and IIB, of ScMreB5 were separately superposed on one of the protofilament of the double protofilament of CcMreB. For superposition Match Maker option in Chimera was used in default settings. Similarly, ScMreB5 subdomains were superposed on other two monomers of the protofilament of CcMreB. This gave a protofilament assembly for ScMreB5.

QUANTIFICATION AND STATISTICAL ANALYSIS

All the statistical analysis and the graphs plotting was performed using the software, GraphPad Prism. Details of statistical tests used, errors bar shown, significance values, the number of independent repeats and the number of cells (n) are mentioned in results, figure legends and also described in the method details.

References

1. Errington, J. (2015). Bacterial morphogenesis and the enigmatic MreB helix. Nat. Rev. Microbiol. *13*, 241–248.
2. Shi, H., Bratton, B.P., Gitai, Z., and Huang, K.C. (2018). How to build a bacterial cell : MreB as the foreman of *E . coli* construction. Cell *172*, 1294–1305.
3. Taylor, J.A., Sichel, S.R., and Salama, N.R. (2019). Bent Bacteria: A

comparison of cell shape mechanisms in *Proteobacteria*. Annu. Rev. Microbiol. *73*, 457–480.

4. Jones, L.J.F., Carballido-López, R., and Errington, J. (2001). Control of cell shape in bacteria: Helical, actin-like filaments in *Bacillus subtilis*. Cell *104*, 913–922.

5. Daniel, R.A., and Errington, J. (2003). Control of cell morphogenesis in bacteria: Two distinct ways to make a rod-shaped cell. Cell *113*, 767–776.

6. Carballido-lópez, R. (2006). Orchestrating bacterial cell morphogenesis. Mol. Microbiol. *60*, 815–819.

7. Carballido-López, R., Formstone, A., Li, Y., Ehrlich, S.D., Noirot, P., and Errington, J. (2006). Actin homolog MreBH governs cell morphogenesis by localization of the cell wall hydrolase LytE. Dev. Cell *11*, 399–409.

8. Shih, Y.-L., and Rothfield, L. (2006). The bacterial cytoskeleton. Microbiol. Mol. Biol. Rev. *70*, 729–754.

9. Ursell, T.S., Nguyen, J., Monds, R.D., Colavin, A., Billings, G., Ouzounov, N., Gitai, Z., Shaevitz, J.W., and Huang, K.C. (2014). Rod-like bacterial shape is maintained by feedback between cell curvature and cytoskeletal localization. Proc. Natl. Acad. Sci. *111*, E1025–E1034.

10. Townsend, R., and Archer, D.B. (1983). A Fibril protein antigen specific to Spiroplasma. J. Gen. Microbiol. *129*, 199–206.

11. Ku, C., Lo, W.-S., and Kuo, C.-H. (2014). Molecular evolution of the actin-like MreB protein gene family in wall-less bacteria. Biochem. Biophys. Res. Commun. *446*, 927–932.

12. Shaevitz, J.W., Lee, J.Y., and Fletcher, D. a. (2005). Spiroplasma swim by a processive change in body helicity. Cell *122*, 941–945.

13. Cohen-Krausz, S., Cabahug, P.C., and Trachtenberg, S. (2011). The monomeric, tetrameric, and fibrillar organization of Fib: the dynamic building block of the bacterial linear motor of *Spiroplasma melliferum BC3*. J. Mol. Biol. *410*, 194–213.
14. Razin, S. (1978). The Mycoplasmas. Microbiol Rev *42*, 414—470.
15. Kürner, J., Frangakis, A.S., and Baumeister, W. (2005). Cryo – electron tomography reveals the cytoskeletal structure of *Spiroplasma melliferum*. Science *307*, 436–439.
16. Trachtenberg, S., Dorward, L.M., Speransky, V. V., Jaffe, H., Andrews, S.B., and Leapman, R.D. (2008). Structure of the cytoskeleton of *Spiroplasma melliferum BC3* and its interactions with the cell membrane. J. Mol. Biol. *378*, 778–789.
17. Wolgemuth, C.W., Igoshin, O., and Oster, G. (2003). The motility of Mollicutes. Biophys. J. *85*, 828–842.
18. Townsend, R., Markham, P.G., Plaskitt, K.A., and Daniels, M.J. (1977). Isolation and characterization of a non-helical strain of *Spiroplasma citri*. J. Gen. Microbiol. *100*, 15–21.
19. Jacob, C., Nouzières, F., Duret, S., Bové, J.M., and Renaudin, J. (1997). Isolation, characterization, and complementation of a motility mutant of *Spiroplasma citri*. J. Bacteriol. *179*, 4802–10.
20. Deeley, J., Stevens, W.A., and Fox, R.T. V. (1979). Use of Dienes' stain to detect plant diseases induced by Mycoplasma-like organisms. Phytopathology *69*, 1169–1171.
21. Wachi, M., Doi, M., Tamaki, S., Park, W., Nakajima-Iijima, S., and Matsuhashi, M. (1987). Mutant isolation and molecular cloning of *mre* genes, which

determine cell shape, sensitivity to mecillinam, and amount of penicillin-binding proteins in *Escherichia coli*. J. Bacteriol. *169*, 4935–4940.

22. Levin, P.A., Margolis, P.S., Setlow, P., Losick, R., and Sun, D. (1992). Identification of *Bacillus subtilis* genes for septum placement and shape determination. J. Bacteriol. *174*, 6717–6728.

23. Figge, R.M., Divakaruni, A. V, and Gober, J.W. (2004). MreB, the cell-shape determining bacterial actin homolog, coordinates cell wall morphogenesis in *Caulobacter crescentus*. Genomics *51*, 1–47.

24. Kruse, T., Bork-Jensen, J., and Gerdes, K. (2005). The morphogenetic MreBCD proteins of *Escherichia coli* form an essential membrane-bound complex. Mol. Microbiol. *55*, 78–89.

25. Altschul, S.F., Gish, W., Miller, W., Myers, E.W., and Lipman, D.J. (1990). Basic local alignment search tool. J. Mol. Biol. *215*, 403–410.

26. Salje, J., van den Ent, F., de Boer, P., and Löwe, J. (2011). Direct membrane binding by bacterial actin MreB. Mol. Cell *43*, 478–487.

27. van den Ent, F., Izoré, T., Bharat, T.A., Johnson, C.M., and Löwe, J. (2014). Bacterial actin MreB forms antiparallel double filaments. Elife *3*, 1–22.

28. Taylor, J.A., Bratton, B.P., Sichel, S.R., Blair, K.M., Jacobs, H.M., Demeester, K.E., Kuru, E., Gray, J., Biboy, J., VanNieuwenhze, M.S., *et al.* (2020). Distinct cytoskeletal proteins define zones of enhanced cell wall synthesis in *Helicobacter pylori*. Elife *9*, 1–38.

29. Cabeen, M.T., Charbon, G., Vollmer, W., Born, P., Ausmees, N., Weibel, D.B., and Jacobs-Wagner, C. (2009). Bacterial cell curvature through mechanical control of cell growth. EMBO J. *28*, 1208–1219.

30. Charbon, G., Cabeen, M.T., and Jacobs-Wagner, C. (2009). Bacterial

intermediate filaments: in vivo assembly, organization, and dynamics of crescentin. Genes Dev. *23*, 1131–1144.

31. Calladine, C.R., Luisi, B.F., and Pratap, J. V. (2013). A “mechanistic” explanation of the multiple helical forms adopted by bacterial flagellar filaments. J. Mol. Biol. *425*, 914–928.

32. Trachtenberg, S. (2004). Shaping and moving a Spiroplasma. J. Mol. Microbiol. Biotechnol. *7*, 78–87.

33. Trachtenberg, S., Gilad, R., and Geffen, N. (2003). The bacterial linear motor of *Spiroplasma melliferum BC3*: from single molecules to swimming cells. Mol. Microbiol. *47*, 671–97.

34. Beven, L., and Wroblewski, H. (1997). Effect of natural amphipathic peptides on viability , membrane potential , cell shape and motility of mollicutes. Res. Microbiol. *148*, 163–175.

35. Strahl, H., and Hamoen, L.W. (2010). Membrane potential is important for bacterial cell division. Proc. Natl. Acad. Sci. U. S. A. *107*, 12281–12286.

36. Nakane, D., Ito, T., and Nishizaka, T. (2020). Co-existence of two chiral helices produces kink translation in Spiroplasma swimming. J. Bacteriol. *202*, e00735-19.

37. Trachtenberg, S. (1998). Mollicutes-wall-less bacteria with internal cytoskeletons. J. Struct. Biol. *124*, 244–256.

38. Waidner, B., Specht, M., Dempwolff, F., Haeberer, K., Schaetzle, S., Speth, V., Kist, M., and Graumann, P.L. (2009). A novel system of cytoskeletal elements in the human pathogen *Helicobacter pylori*. PLoS Pathog. *5*, e1000669.

39. Kruse, T., Mùller-jensen, J., Lùbner-olesen, A., and Gerdes, K. (2003). Dysfunctional MreB inhibits chromosome segregation in *Escherichia coli*.

EMBO J. *22*, 5283–5292.

40. Mauriello, E.M.F., Mouhamar, F., Nan, B., Ducret, A., Dai, D., Zusman, D.R., and Mignot, T. (2010). Bacterial motility complexes require the actin-like protein, MreB and the Ras homologue, MglA. EMBO J. *29*, 315–326.

41. Dempwolff, F., Reimold, C., Reth, M., and Graumann, P.L. (2011). *Bacillus subtilis* MreB orthologs self-organize into filamentous structures underneath the cell membrane in a heterologous cell system. PLoS One *6*.

42. Defeu Soufo, H.J., and Graumann, P.L. (2006). Dynamic localization and interaction with other *Bacillus subtilis* actin-like proteins are important for the function of MreB. Mol. Microbiol. *62*, 1340–1356.

43. Ramond, E., Maclachlan, C., Clerc-Rosset, S., Knott, G.W., and Lemaitre, B. (2016). Cell division by longitudinal scission in the insect endosymbiont *Spiroplasma poulsonii*. MBio *7*, 1–5.

44. Lemoine, F., Correia, D., Lefort, V., Doppelt-Azeroual, O., Mareuil, F., Cohen-Boulakia, S., and Gascuel, O. (2019). NGPhylogeny.fr: New generation phylogenetic services for non-specialists. Nucleic Acids Res. *47*, W260–W265.

45. Letunic, I., and Bork, P. (2019). Interactive Tree of Life (iTOL) v4: Recent updates and new developments. Nucleic Acids Res. *47*, 256–259.

46. Madeira, F., Park, Y. mi, Lee, J., Buso, N., Gur, T., Madhusoodanan, N., Basutkar, P., Tivey, A.R.N., Potter, S.C., Finn, D., *et al.* (2019). The EMBL-EBI search and sequence analysis tools APIs in 2019. Nucleic Acids Res. *47*, 636–641.

47. Solovyev, V., Salamov, A., Seledtsov, I., Vorobyev, D., and Bachinsky, A. (2011). Automatic annotation of microbial genomes and metagenomic sequences. In Metagenomics and its application in agriculture, biomedicine

and environmental studies, Robert W. Li, ed. (Nova Science Publishers, Inc.), pp. 61–78.

48. Vignault, J., Bove, J., Saillard, C., Vogel, R., Farro, A., Venegas, L., Stemmer, W., Aoki, S., McCoy, R., Al-beldawi, A., *et al.* (1980). Mise en culture de spiroplasmes à partir de matériel végétal et d'insectes provenant de pays circum méditerranéens et du Proche Orient. C R Acad Sci Hebd Seances Acad Sci D *290*, 775–778.

49. Duret, S., Andre, A., and Renaudin, J. (2005). Specific gene targeting in *Spiroplasma citri* : improved vectors and production of unmarked mutations using site-specific recombination. Microbiology *151*, 2793–2803.

50. Schneider, C.A., Rasband, W.S., and Eliceiri, K.W. (2012). Image to ImageJ: 25 years of image analysis. Nat. Methods *9*, 671–675.

51. Dubrana, M.P., Guéguéniat, J., Bertin, C., Duret, S., Arricau-Bouvery, N., Claverol, S., Lartigue, C., Blanchard, A., Renaudin, J., and Béven, L. (2017). Proteolytic post-translational processing of adhesins in a pathogenic bacterium. J. Mol. Biol. *429*, 1889–1902.

52. Käll, L., Canterbury, J.D., Weston, J., Noble, W.S., and MacCoss, M.J. (2007). Semi-supervised learning for peptide identification from shotgun proteomics datasets. Nat. Methods *4*, 923–925.

53. Renaudin, J., Béven, L., Batailler, B., Duret, S., Desqué, D., Arricau-bouvery, N., Malembic-maher, S., and Foissac, X. (2015). Heterologous expression and processing of the *Flavescence dorée* phytoplasma variable membrane protein VmpA in *Spiroplasma citri*. BMC Microbiol. *15*, 1–12.

54. Lartigue, C., Duret, S., Garnier, M., and Renaudin, J. (2002). New plasmid vectors for specific gene targeting in *Spiroplasma citri*. Plasmid *48*, 149–159.

55. Stamburski, C., Renaudin, J., and Bove, J.M. (1991). First step toward a virus-derived vector for gene cloning and expression in spiroplasmas, organisms which read UGA as a tryptophan codon: Synthesis of chloramphenicol acetyltransferase in *Spiroplasma citri*. J. Bacteriol. *173*, 2225–2230.
56. Duret, S., Berho, N., Danet, J., Garnier, M., and Renaudin, J. (2003). Spiralin is not essential for helicity, motility, or pathogenicity but is required for efficient transmission of *Spiroplasma citri* by its leafhopper vector *Circulifer haematoceps*. Appl. Environ. Microbiol. *69*, 6225–6234.
57. Duret, S., Danet, J.-L., Garnier, M., and Renaudin, J. (1999). Gene disruption through homologous recombination in *Spiroplasma citri*: An *scm1*-disrupted motility mutant is pathogenic. J. Bacteriol. *181*, 7449–7456.
58. Berho, N., Duret, S., Danet, J., and Renaudin, J. (2006). Plasmid pSci6 from *Spiroplasma citri* GII-3 confers insect transmissibility to the non-transmissible strain *S. citri* 44. Microbiology *152*, 2703–2716.
59. Boudet, J.F., Mathelie-Guinlet, M., Vilquin, A., Douliez, J.P., Béven, L., and Kellay, H. (2018). Large variability in the motility of spiroplasmas in media of different viscosities. Sci. Rep., 1–14.
60. Schneider, T.D., and Stephens, R.M. (1990). Sequence logos: a new way to display consensus sequences. Nucleic Acids Res. *18*, 6097–6100.
61. Kunzelmann, S., and Webb, M.R. (2009). A biosensor for fluorescent determination of ADP with high time resolution. J. Biol. Chem. *284*, 33130–33138.
62. Davis, P.J., Katznel, A., Razin, S., and Rottem, S. (1985). Spiroplasma membrane lipids. J. Bacteriol. *161*, 118–122.
63. Winter, G., Waterman, D.G., Parkhurst, J.M., Brewster, A.S., Gildea, R.J.,

Gerstel, M., Fuentes-Montero, L., Vollmar, M., Michels-Clark, T., Young, I.D., *et al.* (2018). DIALS: Implementation and evaluation of a new integration package. Acta Crystallogr. Sect. D Struct. Biol. *D74*, 85–97.

64. Evans, P.R., and Murshudov, G.N. (2013). How good are my data and what is the resolution? Acta Crystallogr. Sect. D Biol. Crystallogr. *D69*, 1204–1214.

65. Potterton, L., Agirre, J., Ballard, C., Cowtan, K., Dodson, E., Evans, P.R., Jenkins, H.T., Keegan, R., Krissinel, E., Stevenson, K., *et al.* (2018). CCP4i2: The new graphical user interface to the CCP4 program suite. Acta Crystallogr. Sect. D Struct. Biol. *D74*, 68–84.

66. McCoy, A.J., Grosse-Kunstleve, R.W., Adams, P.D., Winn, M.D., Storoni, L.C., and Read, R.J. (2007). Phaser crystallographic software. J. Appl. Crystallogr. *40*, 658–674.

67. Winn, M.D., Ballard, C.C., Cowtan, K.D., Dodson, E.J., Emsley, P., Evans, P.R., Keegan, R.M., Krissinel, E.B., Leslie, A.G.W., McCoy, A., *et al.* (2011). Overview of the CCP4 suite and current developments. Acta Crystallogr. Sect. D Biol. Crystallogr. *D67*, 235–242.

68. Adams, P.D., Afonine, P. V., Bunkóczi, G., Chen, V.B., Davis, I.W., Echols, N., Headd, J.J., Hung, L.W., Kapral, G.J., Grosse-Kunstleve, R.W., *et al.* (2010). PHENIX: A comprehensive Python-based system for macromolecular structure solution. Acta Crystallogr. Sect. D Biol. Crystallogr. *D66*, 213–221.

69. Emsley, P., Lohkamp, B., Scott, W.G., and Cowtan, K. (2010). Features and development of Coot. Acta Crystallogr. Sect. D Biol. Crystallogr. *D66*, 486–501.

70. Rueden, C.T., Schindelin, J., Hiner, M.C., DeZonia, B.E., Walter, A.E., Arena, E.T., and Eliceiri, K.W. (2017). ImageJ2: ImageJ for the next generation of

scientific image data. BMC Bioinformatics *18*.

71. Scheres, S.H.W. (2012). RELION: Implementation of a Bayesian approach to cryo-EM structure determination. J. Struct. Biol. *180*, 519–630.

72. Pettersen, E.F., Goddard, T.D., Huang, C.C., Couch, G.S., Greenblatt, D.M., Meng, E.C., and Ferrin, T.E. (2004). UCSF Chimera - A visualization system for exploratory research and analysis. J. Comput. Chem. *25*, 1605–1612.

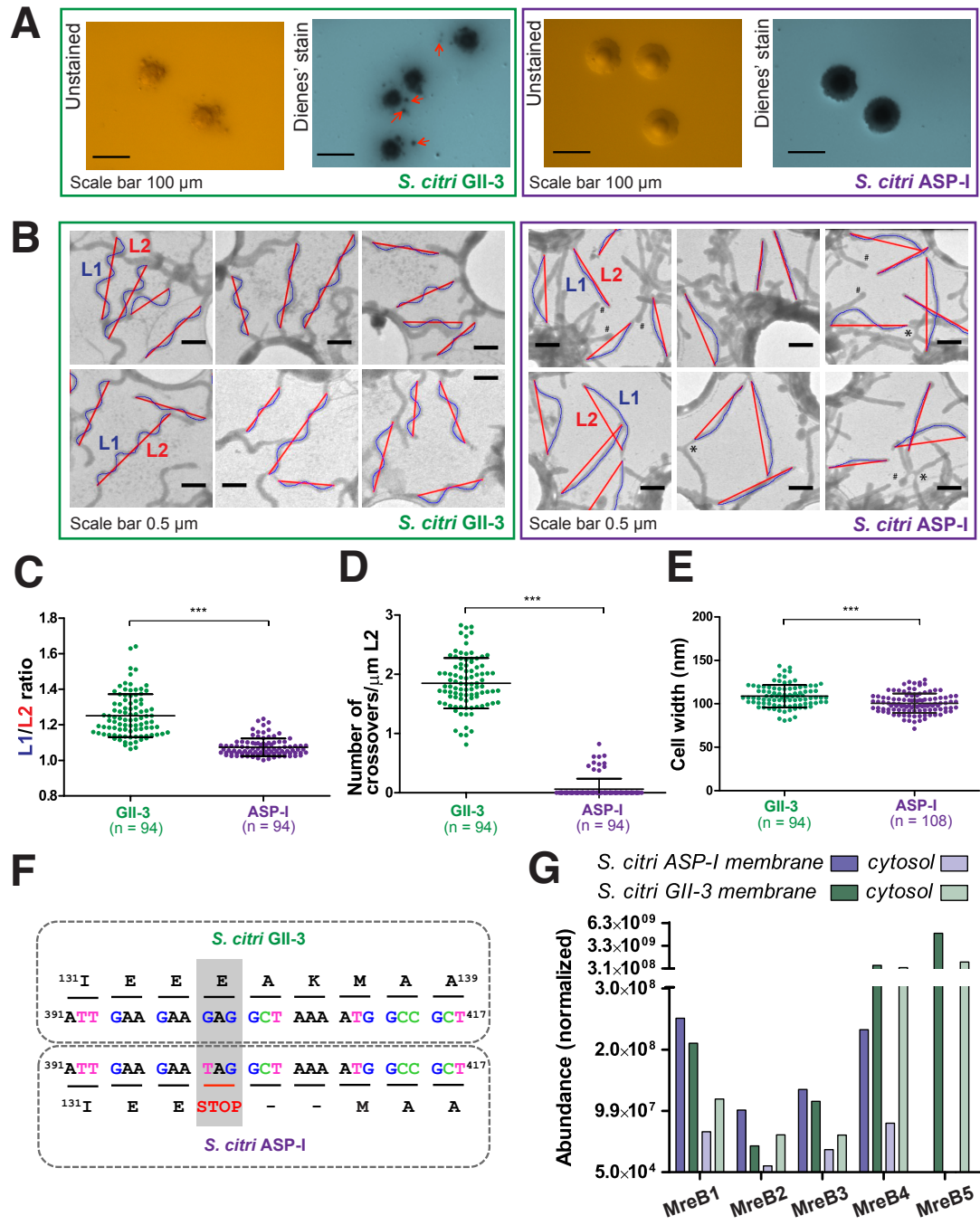
A
Unstained
Dienes' stain
Scale bar 100 µm
S. citri GII-3
Unstained
Dienes' stain
Scale bar 100 µm
S. citri ASP-I
B
L1
L2
Scale bar 0.5 µm
S. citri GII-3
Scale bar 0.5 µm
S. citri ASP-I
C
L1/L2 ratio
***
GII-3 (n = 94)
ASP-I (n = 94)
D
Number of crossovers/µm L2
***
GII-3 (n = 94)
ASP-I (n = 94)
E
Cell width (nm)
***
GII-3 (n = 94)
ASP-I (n = 108)
F
S. citri GII-3
131I E E E A K M A A139
391ATT GAA GAA GAG GCT AAA ATG GCC GCT417
391ATT GAA GAA TAG GCT AAA ATG GCC GCT417
131I E E STOP - - M A A
S. citri ASP-I
G
S. citri ASP-I membrane
cytosol
S. citri GII-3 membrane
cytosol
Abundance (normalized)
6.3×10^09
3.3×10^09
3.1×10^08
3.0×10^8
2.0×10^8
9.9×10^7
5.0×10^4
MreB1
MreB2
MreB3
MreB4
MreB5

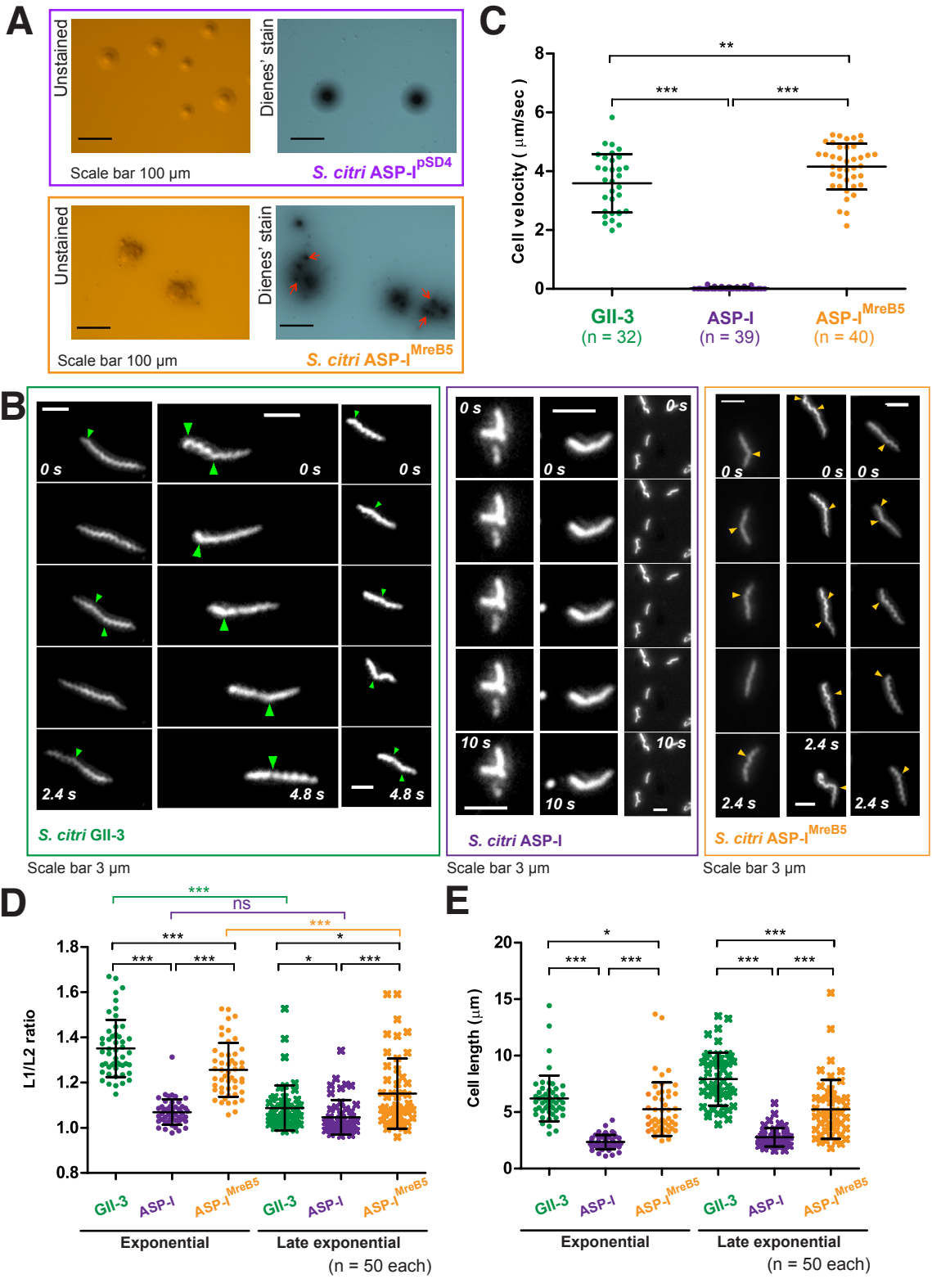
A
Unstained
Dienes' stain
Scale bar 100 µm
S. citri ASP-I pSD4
Unstained
Dienes' stain
Scale bar 100 µm
S. citri ASP-I MreB5
C
Cell velocity (µm/sec)
GII-3
(n = 32)
ASP-I
(n = 39)
ASP-I MreB5
(n = 40)
B
0 s
2.4 s
4.8 s
S. citri GII-3
Scale bar 3 µm
10 s
S. citri ASP-I
Scale bar 3 µm
2.4 s
S. citri ASP-I MreB5
Scale bar 3 µm
D
L1/L2 ratio
GII-3
ASP-I
ASP-I MreB5
Exponential
Late exponential
(n = 50 each)
E
Cell length (µm)
GII-3
ASP-I
ASP-I MreB5
Exponential
Late exponential
(n = 50 each)

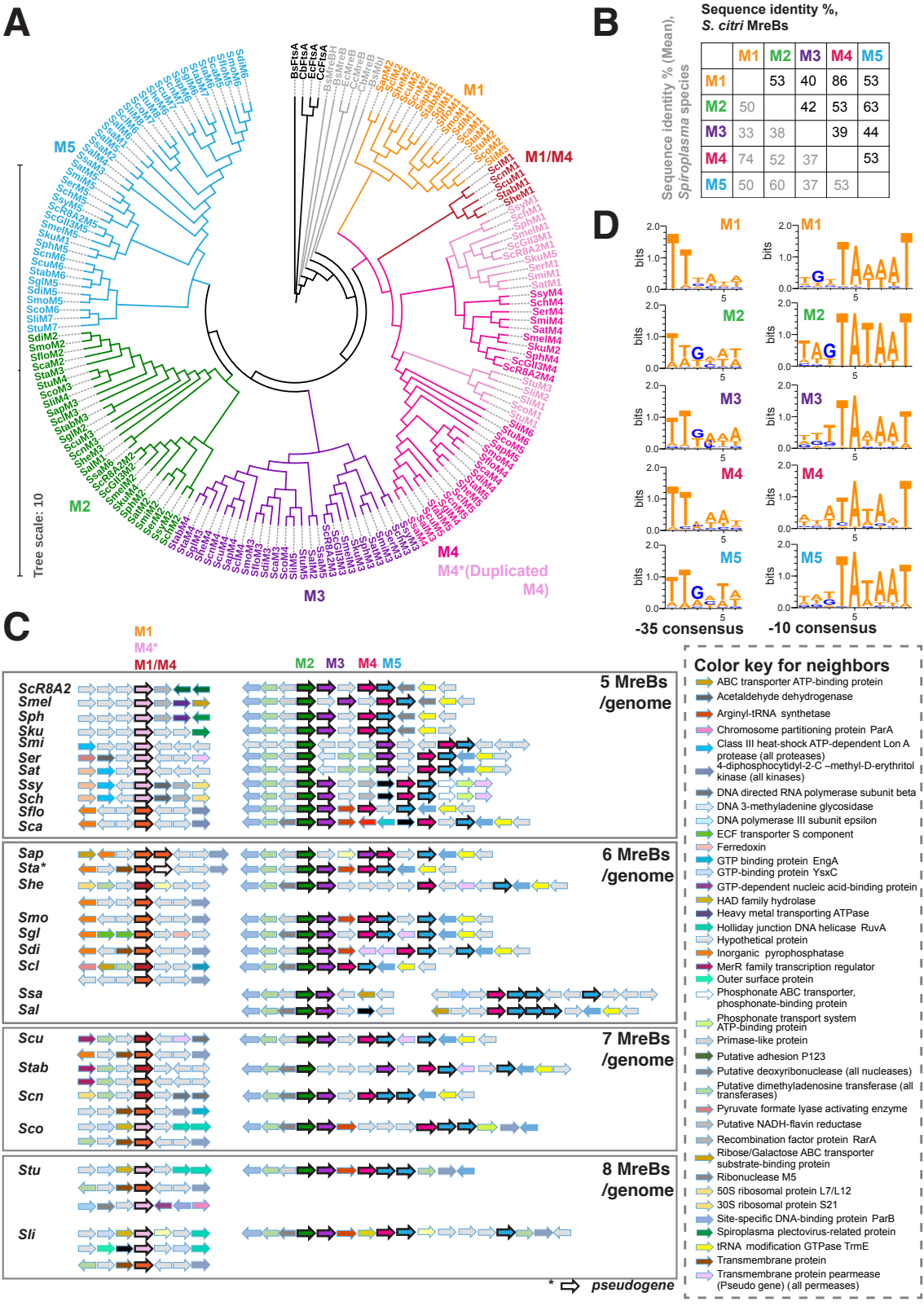
A
M1
M1/M4
M5
M2
M3
M4
M4*(Duplicated M4)
Tree scale: 10
B
Sequence identity %, S. citri MreBs
Sequence identity % (Mean), Spiroplasma species
M1 M2 M3 M4 M5
M1 53 40 86 53
M2 50 42 53 63
M3 33 38 39 44
M4 74 52 37 53
M5 50 60 37 53
D
M1
M2
M3
M4
M5
bits
-35 consensus
-10 consensus
C
M1
M4*
M1/M4
M2 M3 M4 M5
ScR8A2
Smel
Sph
Sku
Smi
Ser
Sat
Ssy
Sch
Sflo
Sca
5 MreBs /genome
Sap
Sta*
She
Smo
Sgl
Sdi
Scl
Ssa
Sal
6 MreBs /genome
Scu
Stab
Scn
Sco
7 MreBs /genome
Stu
Sli
8 MreBs /genome
* pseudogene
Color key for neighbors
ABC transporter ATP-binding protein
Acetaldehyde dehydrogenase
Arginyl-tRNA synthetase
Chromosome partitioning protein ParA
Class III heat-shock ATP-dependent Lon A protease (all proteases)
4-diphosphocytidyl-2-C –methyl-D-erythritol kinase (all kinases)
DNA directed RNA polymerase subunit beta
DNA 3-methyladenine glycosidase
DNA polymerase III subunit epsilon
ECF transporter S component
Ferredoxin
GTP binding protein EngA
GTP-binding protein YsxC
GTP-dependent nucleic acid-binding protein
HAD family hydrolase
Heavy metal transporting ATPase
Holliday junction DNA helicase RuvA
Hypothetical protein
Inorganic pyrophosphatase
MerR family transcription regulator
Outer surface protein
Phosphonate ABC transporter, phosphonate-binding protein
Phosphonate transport system ATP-binding protein
Primase-like protein
Putative adhesion P123
Putative deoxyribonuclease (all nucleases)
Putative dimethyladenosine transferase (all transferases)
Pyruvate formate lyase activating enzyme
Putative NADH-flavin reductase
Recombination factor protein RarA
Ribose/Galactose ABC transporter substrate-binding protein
Ribonuclease M5
50S ribosomal protein L7/L12
30S ribosomal protein S21
Site-specific DNA-binding protein ParB
Spiroplasma plectovirus-related protein
tRNA modification GTPase TrmE
Transmembrane protein
Transmembrane protein pearmease (Pseudo gene) (all permeases)

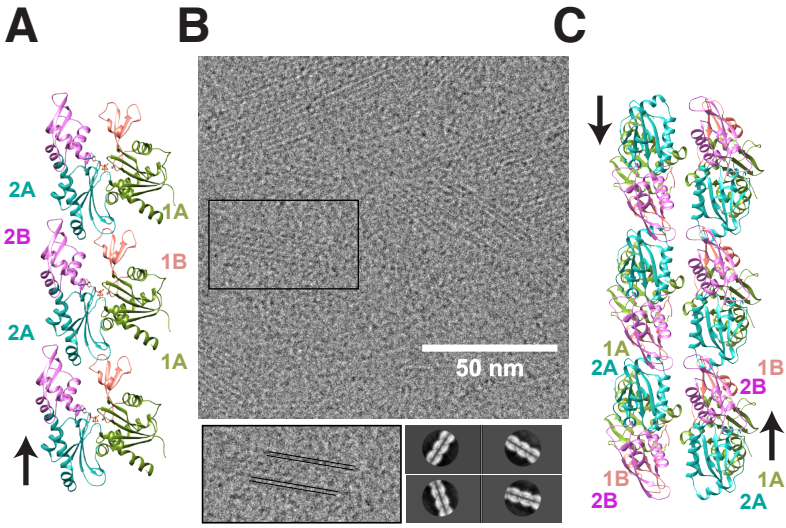
A
B
C
2A
2B
1A
1B
2A
1A
50 nm
1A
2A
1B
2B
1B
2B
1A
2A

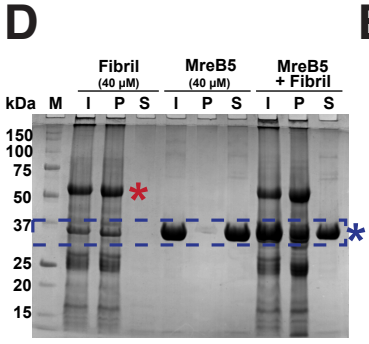
D
Fibril
(40 μM)
MreB5
(40 μM)
MreB5
+ Fibril
kDa M I P S I P S I P S
150
100
75
50
37
25
20
15

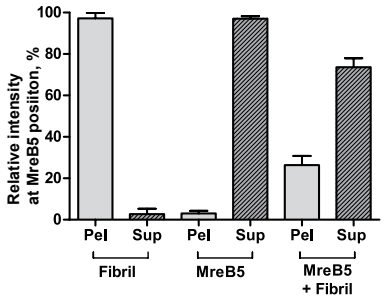
E
Relative intensity
at MreB5 positon, %
100
80
60
40
20
0
Pel
Sup
Pel
Sup
Pel
Sup
Fibril
MreB5
MreB5
+ Fibril

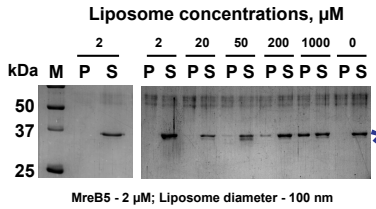
F
Liposome concentrations, μM
2
2
20
50
200
1000
0
kDa M P S P S P S P S P S P S P S
50
37
25
MreB5 - 2 μM; Liposome diameter - 100 nm

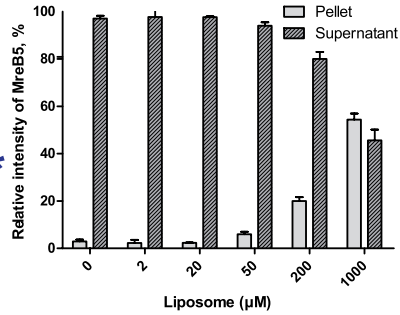
G
Pellet
Supernatant
Relative intensity of MreB5, %
100
80
60
40
20
0
0
2
20
50
200
1000
Liposome (μM)

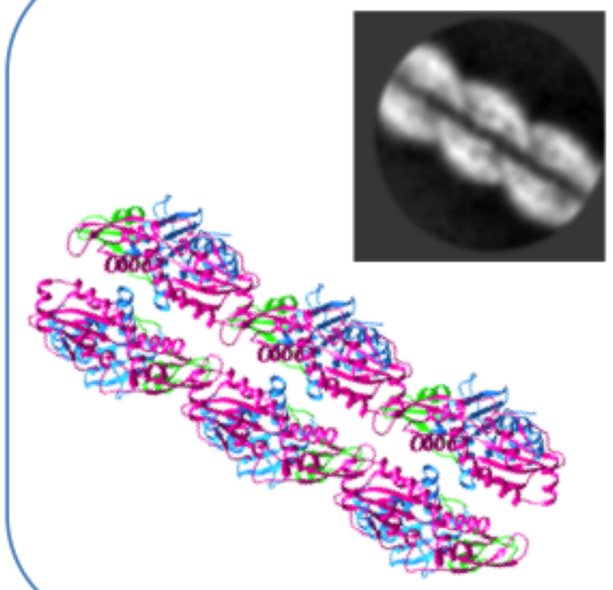

MreB5

Antiparallel double protofilaments

Binds liposomes

Binds fibril

+ MreB5

Non-helical and Non-motile

Helical and Motile